Received: 27 January 2024 | Revised: 8 April 2024 | Accepted: 9 April 2024

DOI: 10.1002/chir.23673

RESEARCH ARTICLE

Chirality WILEY

Impact of helical elongation of symmetric oxa[*n*]helicenes on their structural, photophysical, and chiroptical characteristics

Mohamed S. H. Salem[1,2] | **Rubal Sharma**[1,3] | **Seika Suzuki**[4] | **Yoshitane Imai**[4] | **Mitsuhiro Arisawa**[3] | **Shinobu Takizawa**[1]

[1]SANKEN, Osaka University, Osaka, Japan

[2]Pharmaceutical Organic Chemistry Department, Faculty of Pharmacy, Suez Canal University, Ismailia, Egypt

[3]Graduate School of Pharmaceutical Sciences, Osaka University, Osaka, Japan

[4]Department of Applied Chemistry, Faculty of Science and Engineering, Kindai University, 3-4-1 Kowakae, Osaka, Higashi-Osaka, Japan

Correspondence
Dr. M.S.H. Salem and Prof. S. Takizawa, SANKEN, Osaka University, Mihogaoka, Ibaraki-shi, Osaka 567-0047, Japan.
Email: mohamedsalem43@sanken.osaka-u.ac.jp and taki@sanken.osaka-u.ac.jp

Funding information
Ministry of Education, Culture, Sports, Science, and Technology (MEXT), Grant/Award Numbers: 24K17681, 21A204, 21H05217, 22K06502; Japan Society for the Promotion of Science (JSPS); Core Research for Evolutionary Science and Technology (JST CREST), Grant/Award Number: JPMJCR20R1; Hoansha Foundation

Abstract

The adjustment of the main helical scaffold in helicenes is a fundamental strategy for modulating their optical features, thereby enhancing their potential for diverse applications. This work explores the influence of helical elongation (n = 5–9) on the structural, photophysical, and chiroptical features of symmetric oxa[*n*]helicenes. Crystal structure analyses revealed structural variations with helical extension, impacting torsion angles, helical pitch, and packing arrangements. Through theoretical investigations using density functional theory (DFT) calculations, the impact of helical extension on aromaticity, planarity distortion, and heightened chiral stability were discussed. Photophysical features were studied through spectrophotometric analysis, with insights gained through time-dependent DFT (TD-DFT) calculations. Following optical resolution via chiral high-performance liquid chromatography (HPLC), the chiroptical properties of both enantiomers of oxa[7]helicene and oxa[9]helicene were investigated. A slight variation in the main helical scaffold of oxa[*n*]helicenes from [7] to [9] induced an approximately three-fold increase in dissymmetry factors with the biggest values of $|g_{lum}|$ of oxa[9]helicene (2.2×10^{-3}) compared to $|g_{lum}|$ of oxa[7]helicene (0.8×10^{-3}), findings discussed and supported by TD-DFT calculations.

KEYWORDS

chiroptical, circular dichroism, circularly polarized luminescence, crystal analysis, enantiomerization barrier, helical elongation, helicene, time-dependent DFT

1 | INTRODUCTION

Helicenes are *ortho*-fused polycyclic aromatic hydrocarbons in which the aromatic rings are angularly annulated to give them their characteristic helical scaffold.[1–3] This unique structure with an extended π-conjugated system and inherent chirality imparts various desirable electronic, photophysical, and chiroptical properties,

This article is a contribution to the special issue "Proceedings of 19th International Conference on Chiroptical Spectroscopy, Hiroshima, Japan 2023."

including circular dichroism (CD) and circularly polarized luminescence (CPL).[4–6] Exploiting these advantages, helicenes have found applications in diverse material fields, such as molecular sensors,[7,8] chiral switches,[9] bioimaging, quantum computers, and displays.[10] Extensive efforts have been devoted to enhancing the optical properties of helicenes, with a focus on studying the impact of structural modifications on these properties. Many reports have delved into the substituents' effects on the chiroptical features of various hetero-,[11] carbo-,[12,13] and expanded helicenes[14] revealing improved performance with specific moieties (e.g. maleimide),[15] or patterns (e.g. push-pull).[16] Heteroatoms doping into helicenes, to modulate their characteristics, has been explored with many successful examples.[17–20] Moreover, the introduction of certain motifs (e.g. binaphthyl) as a hinge,[21] creating helicenes with multiple helicities,[22] or symmetric architecture showed superior chiroptical behavior.[23]

Notably, the tuning of the main helical scaffold either by truncation[24] or extension is one of the key tools to modulate the optical behavior of these structures. Recently, the impact of both lateral and helical π-extensions on the chiroptical properties of helicenes has been studied through some examples showing significant amplification of their dissymmetry factors ($|g_{abs}|$and$|g_{lum}|$).[25–27] In 2012, Mori and Inoue conducted a pioneering theoretical and experimental study on the helical extension-CD relationship through a series of carbo[*n*]helicenes (n = 4–10).[28] This study initiated further investigations, introducing efficient strategies for helical chain elongation and examining its impact on CD.[29–31] The exploration of lateral and helical extension effects on CPL, however, lagged until recent times. Few studies delved into the influence of lateral π-extension with specific moieties (e.g., naphthalimides) on CPL.[32,33] In 2021, Pieters, Müllen, and Narita explored the effects of helical elongation of some π-extended carbo[*n*]helicenes (n = 7, 9), revealing that a small variation in helical length from (n = 7) to (n = 9) caused an approximately 10-fold increase in dissymmetry factors (Figure 1A).[34] In 2022, Nowak-Król investigated a specific class of azabora[*n*]helicenes (n = 5–7), highlighting the positive impact of both lateral and helical extensions on chiroptical responses (Figure 1B).[35] In 2023, Martín presented a different scenario where the helical extension of bilayer nanographene with a helicene core weakened the overlapping degree between these two π-extended layers, resulting in a drop in photophysical and chiroptical properties (Figure 1C).[36]

Despite these recent valuable studies, this area is still underexplored, as most of the effort mainly focused on carbo[*n*]helicenes[32–34,36] or was confined to computational investigations without any experimental study.[27,37,38] Most of the examples involved specific types of π-extended helicenes with complex scaffolds, making it challenging to generalize their conclusions. Inspired by our prior works,[39–43] and encouraged by their advantageous short-step synthesis and characteristics, we built our study on symmetric oxa[*n*]helicenes. Oxa[*n*]helicenes, particularly those with furan rings, show many advantages related to their ease of synthesis from simple building blocks within two steps including oxidative coupling followed by dehydrative cyclization. Additionally, they exhibited high luminescence compared to other hetero[*n*]helicenes due to their elevated HOMO levels.[44–46] Therefore, we conducted a theoretical and computational analysis to examine the impact of helical extension on a series of previously reported symmetric oxa[*n*]helicenes (*n* = 5–9) on their structural, photophysical, and chiroptical properties (Figure 1D).

2 | MATERIALS AND METHODS

2.1 | General

All simple chemicals and solvents were purchased from commercial suppliers and used without further purification. UV–Vis absorption spectra were obtained on a Jasco V−670 spectrophotometers. CD spectra were recorded on a Jasco J−1700 spectropolarimeter. Emission spectra were obtained on an FP − 8,650 spectrometer. CPL spectra were obtained at room temperature using a JASCO CPL − 300 spectrofluoropolarimeter (Tokyo, Japan). The absolute PL quantum yields were measured using an Absolute PL Quantum Yield Measurement System (C9920–02, Hamamatsu Photonics [Hamamatsu, Japan]) in the air at room temperature.

2.2 | DFT calculations

All DFT calculations were performed using the Gaussian 16 and Gaussian 9 packages of programs.[47,48] The geometries of the structures of oxa[*n*]helicenes **OH5**, **OH7**, and **OH9** were optimized at both the ground S_0 and excited S_1 states calculated with MN15/6-311G(d,p)/PCM = chloroform level of theory.[49] All stationary points were identified as stable minima by frequency calculations and the geometry optimization was achieved using the normal criteria in Gaussian software. The nucleus-independent chemical shift (NICS)[50,51] indices were calculated in the centrum of each ring NICS(0) and 1 Å above/below the centrum NICS(1) within gauge-independent atomic orbital (GIAO) approximation at MN15/6-311G(d,p) and B3LYP/6-311G(d,p) levels of theory.[52] For the anisotropy of the induced current density (AICD) simulations, the

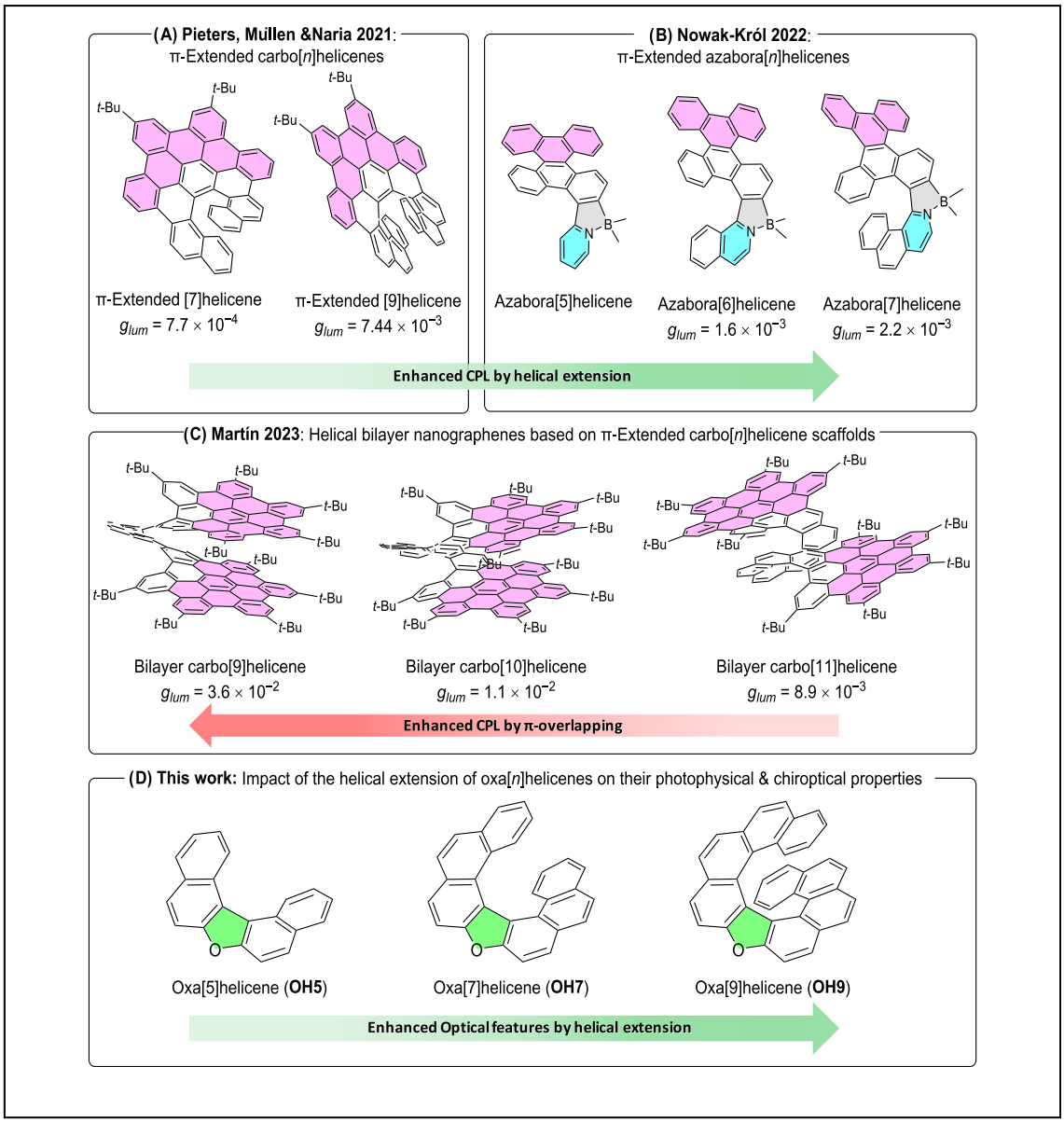

FIGURE 1 Impact of the helical extension of [*n*]helicenes on their optical features.

AICD-3.0.4 software was used.[53] The enantiomerization barriers were studied using MN15 as a functional and 6-311G(d,p) as a basis set.[54] TD-DFT calculations were performed directly on cartesian coordinates obtained from the crystal structures of oxa[*n*]helicenes at MN15/6-311G(d,p)/PCM = chloroform level of theory and on those optimized at the lowest energy singlet excited state (S_1).[55] The electric and magnetic transition dipole moments of **OH5**, **OH7**, and **OH9** were calculated by Multiwfn[56] and visulaized using VMD software.[57] For further computational details, (see Section 7, Supporting Information).

3 | RESULTS AND DISCUSSION

3.1 | Synthetic procedures of OH5, OH7, and OH9

In order to investigate the optical characteristics of symmetric oxa[*n*]helicenes featuring differing quantities of angularly annulated benzene rings in the *ortho* configuration, We synthesized three previously reported examples.[39,58,59] Oxa[5]helicene **OH5** was synthesized smoothly from commercially available *rac*-BINOL through an acid-promoted dehydrative cyclization.[58] Employing a

similar strategy, we synthesized oxa[7]helicene **OH7** from the corresponding 4,4′-biphenanthryl-3,3′-diol. Through a comprehensive screening of different acid additives (Table S1, see Supporting Information), we discerned that this synthetic approach yielded **OH7** with enhanced overall yield and a reduced number of steps.[59] For the enantioselective synthesis of oxa[9]helicene **OH9**, we employed our developed method of enantioselective sequential synthesis of oxa[9]helicenes catalyzed by a chiral vanadium complex (see Supporting Information).[39]

3.2 | Effects of helical elongation on the structures of oxa[*n*]helicenes

To understand the inherent structural characteristics and packing arrangements of symmetric oxa[*n*]helicenes, we conducted a comparative study. We analyzed the crystal structures of **OH9**, in comparison with **OH7** and **OH5** that our group, along with the Nozaki and Xu groups, previously crystallized and deposited in the Cambridge Crystallographic Data Centre (CCDC). These samples were crystallized in space groups $P2_1$ (**OH9**), Pbca (**OH7**), and P1 (**OH5**) under deposition numbers of CCDC-1493624, CCDC-280431, and CCDC-1877578, respectively (Figure 2A). The torsion angles in **OH5** and **OH7** exhibited similar values, measuring 14.72° for (atoms a − b − c − d) and 17.88° for (atoms a′ − b′ − c’ − d′). In contrast, the corresponding angle in **OH9** was smaller at 4.67° for (atoms a“ − b” − c” − d”) due to the overlapping of benzene rings. The sums of all dihedral angles of the inner helicene rims (φ) were 34.70°, 78.93°, and 125.06° for **OH5**, **OH7**, and **OH9**, respectively, with an average of (11.57°, 15.79°, and 17.87°). This indicated a more distorted structure for **OH9**, as evident in the increasing pattern of torsion angles between the centroids of terminal rings with the helical extension, measuring 72.8° (**OH9**) compared to 16.6°, and 36.7° for **OH5** and **OH7**, in turn (Figure 2A). The helical pitch, determined from the centroid−centroid distance of the overlapping benzene rings, measured 3.95 Å for **OH7**, while it was 3.53 Å and 3.66 Å between (A′ and B′ centroids) in **OH9**. The packing arrangement of oxa[*n*]helicenes was governed to a large extent by multiple C − H···π interactions between the neighboring molecules of the same or opposite chirality (Figure 2B).

3.3 | Effects of helical extension on the aromaticity

Subsequently, we employed nucleus-independent chemical shifts (NICS), proposed by Schleyer and colleagues, as a magnetic indicator for studying how chain elongation can affect aromaticity.[50,51] As depicted in Figure 3A, the aromaticity of terminal rings exhibited a progressive

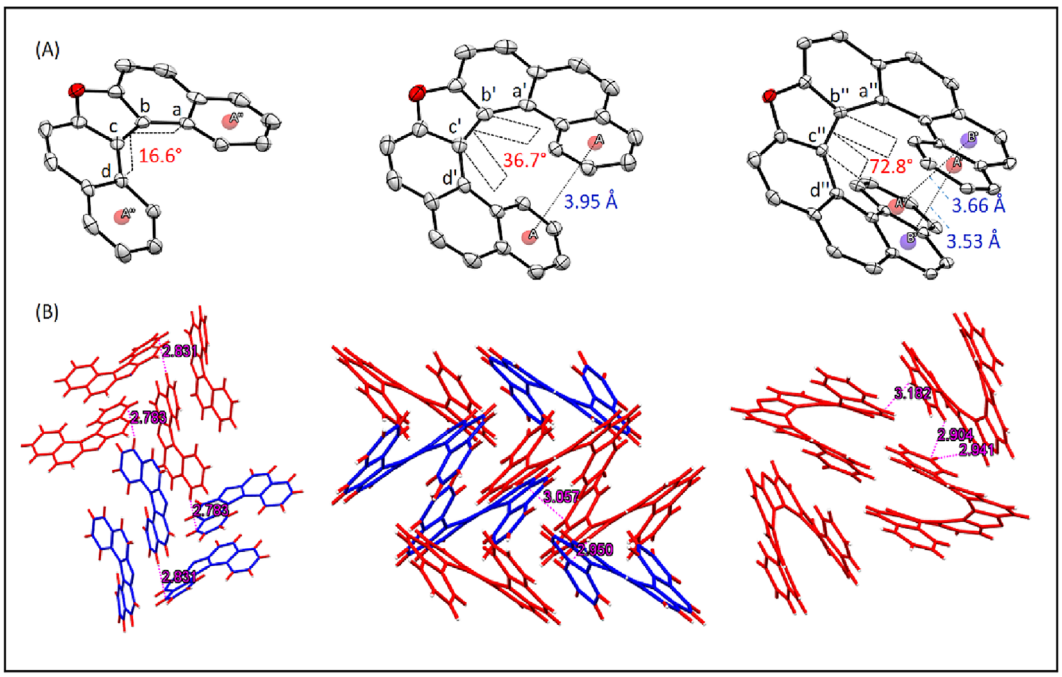

FIGURE 2 X-ray crystal analysis: (A) single-crystal structures of (*M*)-**OH5**, (*M*)-**OH7**, and (*M*)-**OH9** with ellipsoids at 30% probability (H atoms were omitted for clarity); (B) molecular packing of **OH5** (viewed along a-axis), **OH7 and OH9** (viewed along b-axis), red color represents (*M*)-configuration and blue color represents (*P*)-configuration.

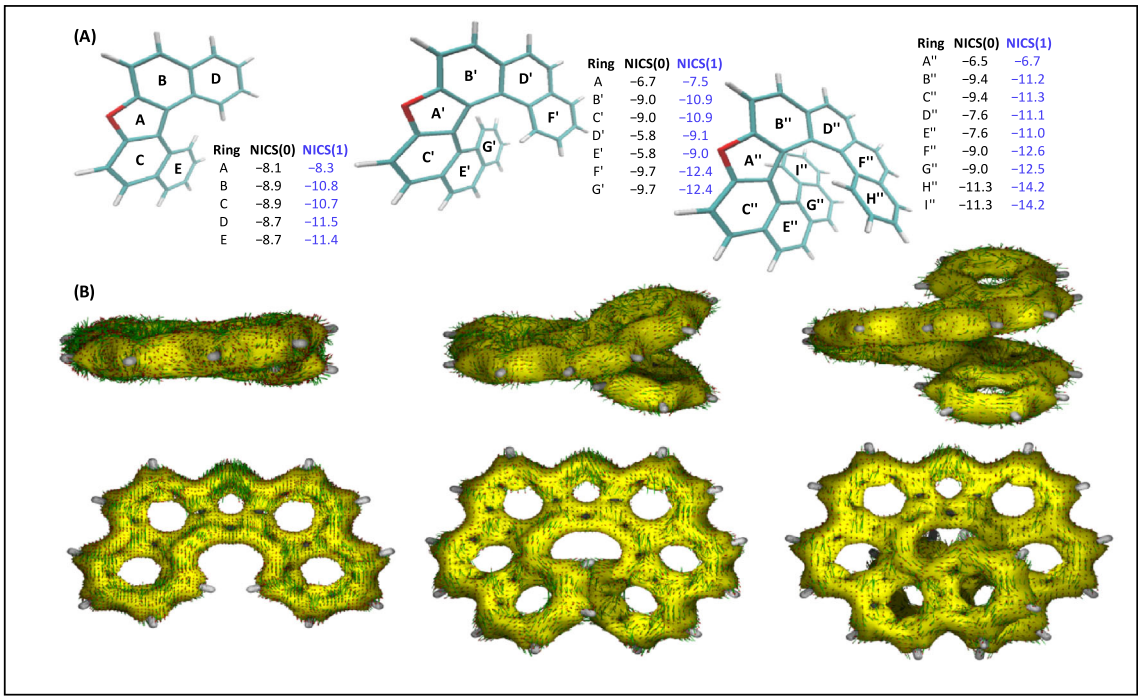

FIGURE 3 Aromaticity of symmetric oxa[*n*]helicenes: (A) NICS(0) and NICS(1) values of **OH5**, **OH7**, and **OH9** calculated at the MN15/6-311G(d,p) level of theory; (B) ACID plots calculated at the B3LYP/6-311G(d,p) level of theory (isosurface value: 0.05).

augmentation with helical elongation, evidenced by NICS(1) values of −11.5 and −11.4 (rings D and E, **OH5**), −12.4 (rings F′ and G′, **OH7**), and −14.2 (rings H″ and I″, **OH9**). This can be ascribed to the magnetic interplay between the superimposed rings, elucidated through the Johnson-Bovey model, since the distance between rings is approximately 3.5–4.0 Å (Figure 2A).[60] On the other hand, the aromaticity of central furan rings (A, A′, and A″) decreased with helical elongation. This trend aligned with some previous observations in other classes of polyacenes during NICS calculations, prompting researchers sometimes to interpret it as an overestimation of NICS for the local aromaticity of central rings.[61] The main reason behind this decline in aromaticity is the distortion in planarity of the furan cores with helical elongation, a phenomenon supported by precedent studies on carbo[*n*]helicenes.[61] Similarly, the distortion in planarity elucidated the decreased aromaticity of some rings (e.g. rings D′ and E′ of **OH7**, and rings D″ and E″ of **OH9**) relative to other benzene rings (Figure 3A). To gain further insights, we conducted the anisotropy of the induced current density (AICD) calculations for **OH5**, **OH7**, and **OH9** at the B3LYP/6-311G(d,p) level of theory in the gas phase (Figure 3B).[53] The plot revealed a clockwise current flowing along the fused furan and benzene rings, aligning with those reported in other helicene scaffolds, typically characterized by diatropic ring currents.[62]

3.4 | Photophysical properties of the oxa[*n*]helicenes

The absorption and emission spectra of **OH5**, **OH7**, and **OH9** in chloroform solutions (1×10^{-5} M) were studied and are presented in Figures 4A and B. The extended helical length of **OH9**, denoted as *n*, imparted greater π-conjugation compared to **OH7** and **OH5**, evident from the red-shifted absorption and emission bands. In chloroform, **OH5** exhibited a noteworthy absorbance peak at 356 nm with an absorption coefficient of ($\varepsilon = 3.1 \times 10^4$ $M^{-1}{\cdot}cm^{-1}$), and an optical bandgap ($E_g = 3.44$ eV). Similarly, **OH7** and **OH9** displayed their highest absorbances at 388 nm ($\varepsilon = 1.3 \times 10^4$ $M^{-1}{\cdot}cm^{-1}$) and 404 nm ($\varepsilon = 1.2 \times 10^4$ $M^{-1}{\cdot}cm^{-1}$), with optical bandgaps (E_g) of 3.13 eV and 3.02 eV, respectively (more details in Supporting Information). The photoluminescence (PL) spectra of oxa[*n*]helicenes were recorded in pure chloroform and demonstrated bathochromic shifts with emission maxima at 362 and 380 nm for **OH5**, 398 and 416 nm for **OH7**, and 411 and 432 nm for **OH9**. Employing time-dependent density functional theory (TD-DFT) calculations, we investigated the electronic transition properties of **OH5**, **OH7**, and **OH9** upon optimizing their molecular structures at the lowest energy singlet excited state (S_1).[63,64] The convergence of these optimized structures was confirmed through frequency analysis, showing

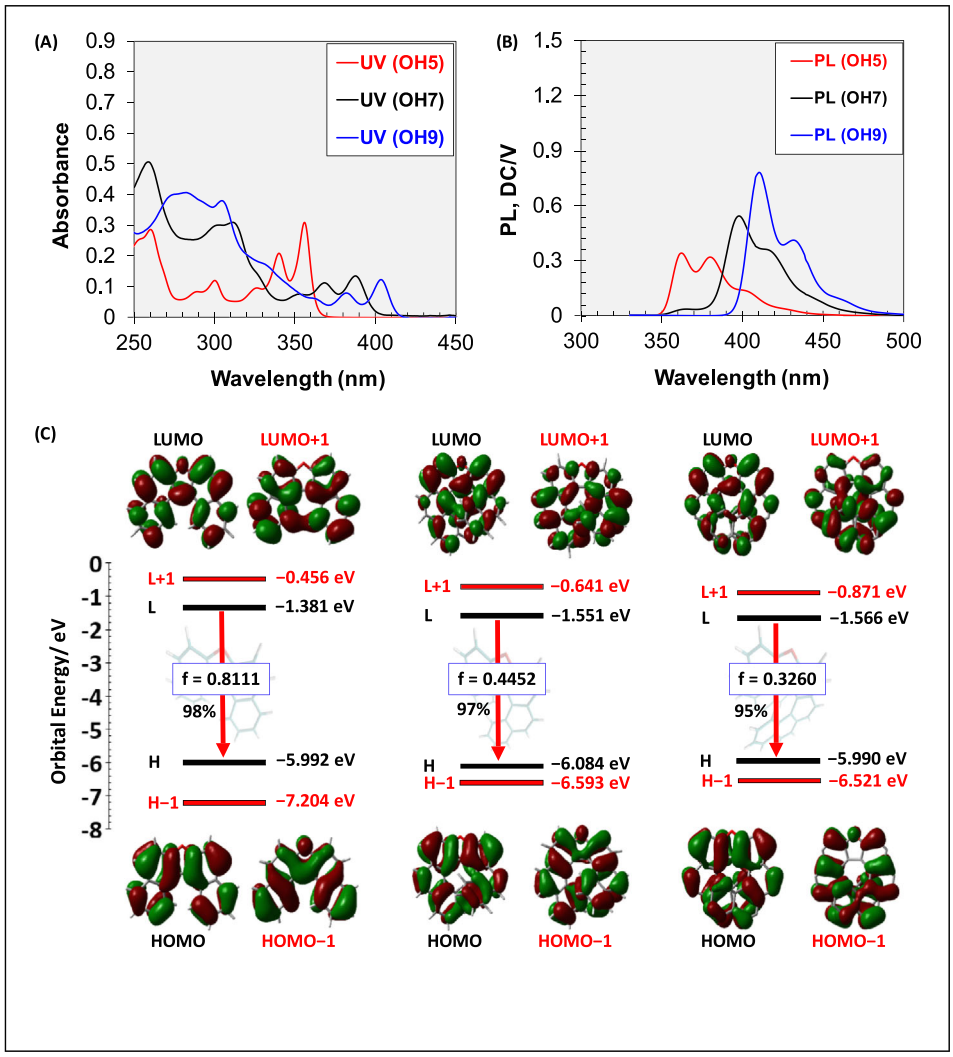

FIGURE 4 Photophysical characters of oxa[*n*]helicenes **OH5**, **OH7**, and **OH9**: (A) & (B) UV/Vis absorption and PL spectra in chloroform (Conc = 1×10^{-5} M); (C) Frontier Kohn-Sham molecular orbitals (HOMO & LUMO) of **OH5**, **OH7**, and **OH9** optimized in the lowest energy excited state (S_1) and TD-DFT calculated transitions at MN15/6-311G(d,p)/PCM = chloroform level of theory.

no imaginary frequencies. The frontier orbitals of symmetric oxa[*n*]helicenes (n = 5–9) are not degenerate, and only the LUMO → HOMO transitions contribute to the $S_1 \rightarrow S_0$ transitions. Oscillator strength of the $S_1 \rightarrow S_0$ transitions decreases with helical elongation, which can be attributed to the reduced orbital degeneracy of **OH5** compared to **OH7** and **OH9** (Figure 4C).

Generally, most unsubstituted carbo[*n*]helicenes ($n \geq 5$) exhibit small quantum yields ($\Phi_f < 5\%$) due to the low oscillator strength of their $S_1 \rightarrow S_0$ transitions.[65] The fluorescence quantum yields (in chloroform solutions 1×10^{-3} M) of **OH5** ($\Phi_f = 10.7\%$) and **OH7** ($\Phi_f = 11.2\%$) were three times higher than that of **OH9** ($\Phi_f = 3.8\%$), which can be attributed to their increased radiative rate constants (k_f). The theoretically determined $k_{f,calcd}$ values were 0.497, 0.160, and 0.076 ns^{-1} for **OH5**, **OH7**, and **OH9**, respectively (further details in Table S25, ESI). According to the equation $\Phi_f = k_f/(k_f + k_{nr})$, which relates the quantum yield to two decay constants k_f and *the* nonradiative decay constant k_{nr}, the higher $k_{f,calcd}$ values of **OH5** and **OH7** compared to **OH9** can explain their higher quantum yields.[66,67]

3.5 | Enantiomerization barriers of oxa[*n*]helicenes

To explore the enantiomerization barriers (*P*/*M*) of **OH5**, **OH7**, and **OH9**, we employed DFT calculations to identify the transition states with the highest Gibbs free energies. These states featured a face-to-face orientation of the terminal rings in the helix, as depicted in Figure 5. The enantiomerization barriers of **OH5**, **OH7**, and **OH9** were calculated to be 3.18, 33.56, and 44.46 kcal mol^{-1}, respectively. These values closely align with those reported for other helicenes,[34,42,68,69] underscoring the significant influence of helical π-extension on the rigidity of the helical backbones. Notably, the remarkably high (*P*/*M*) enantiomerization barrier for **OH9** contributed to the exceptional thermal stability of its enantiomers,

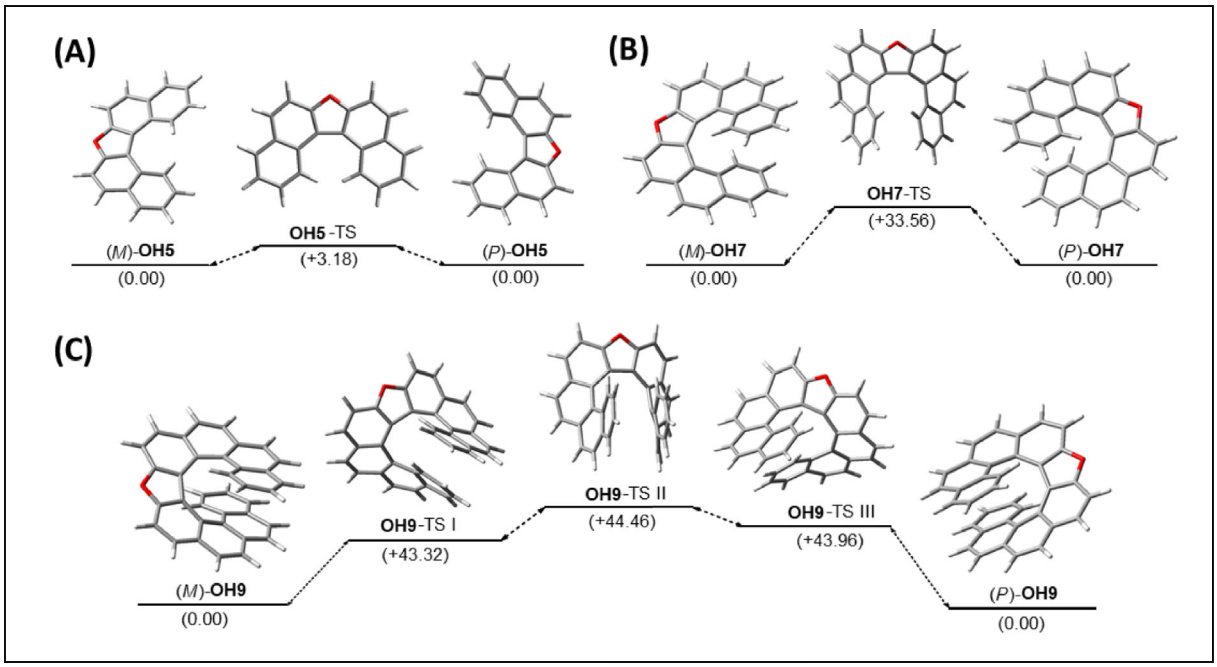

FIGURE 5 (*P*/*M*) Enantiomerization process of **OH5** (A), **OH7** (B), and **OH9** (C); relative Gibbs free energies were calculated in (kcal Mol^{-1}) at the MN15/6-311G(d,p) level of theory.

observed when solutions of (*M*)-**OH9** were heated at 150 °C for 2 hours without any racemization. These results also compare well with the experimentally determined enantiomerization barrier of (*P*)-**OH9** (~40 kcal mol^{-1}) as reported by Hossain and Karikomi using an Eyring plot.[70]

3.6 | Effects of helical elongation on the chiroptical features of oxa[*n*]helicenes

Due to the rapid racemization of (*P*/*M*)-**OH5** at ambient temperature, achieving chiral resolution for both enantiomers proved to be exceptionally challenging. In contrast, the higher enantiomerization barriers of (*P*/*M*)-**OH7** and (*P*/*M*)-**OH9** facilitated the complete resolution of their enantiomers through HPLC, employing a Daicel Chiralpak IA column (Figure S4, see Supporting Information). CD spectra of isolated enantiomers (*P*/*M*)-**OH7** and (*P*/*M*)-**OH9** in chloroform solutions (1×10^{-5} M) were measured (Figure 6A). To assign the configuration of each isomer, we compared the obtained CD spectra to those derived from TD-DFT calculations (refer to Supporting Information) and the previously reported CD spectra of **OH9** by Hossain and Karikomi.[70] The absolute configurations in the first and second fractions of the chiral HPLC analysis were designated as the (*P*)- and (*M*)-enantiomers, respectively, for both **OH7** and **OH9**. Interestingly, due to the increase in helical length (*n*) from 7 to 9, **OH9** exhibited a significantly higher $\Delta\varepsilon$ than **OH7** in the long-wavelength region. CD spectra revealed $|g_{abs}|$ values for **OH7** as 4.6×10^{-3} and 1.8×10^{-3} at $\lambda_{abs} = 319$ and 268 nm, respectively and $|g_{abs}|$values for **OH9** as 1.6×10^{-3}, 5.3×10^{-3}, 8.0×10^{-3}, 4.4×10^{-3}, and 3.9×10^{-3} at $\lambda_{abs} = 405$, 353, 316, 300, and 269 nm, in turn, for both enantiomers (Table 1). The higher values of g_{abs} for **OH9** were further supported by simulated CD spectra (Figure S16, see Supporting Information).

Subsequently, CPL spectra of (*P*/*M*)-**OH7** and (*P*/*M*)-**OH9** were measured to explore the potential of these oxa[*n*]helicenes as chiral emitters. The $|g_{lum}|$values were measured as 0.81×10^{-3} at 402 nm for **OH7** and 2.2×10^{-3} at 413 nm for **OH9**, with the (*P*)-configuration exhibiting a positive Cotton effect and the (*M*)-configuration displaying a negative Cotton effect (Figure 6A). According to theory,[71,72] g_{lum} can be determined by the following eq. 1:

$$|g| = \frac{4.|\mu|.|m|.\cos\theta_{\mu,m}}{|\mu|^2 + |m|^2} \quad (1)$$

Therefore, the electric (μ) and magnetic (m) transition dipole moments, as well as the angle (θ) between μ and m, of (*M*)-**OH5**, (*M*)-**OH7**, and (*M*)-**OH9** for their $S_1 \rightarrow S_0$ transitions were determined using TD-DFT calculations (Figure 6B).[73,74] For organic materials, the |m| value is

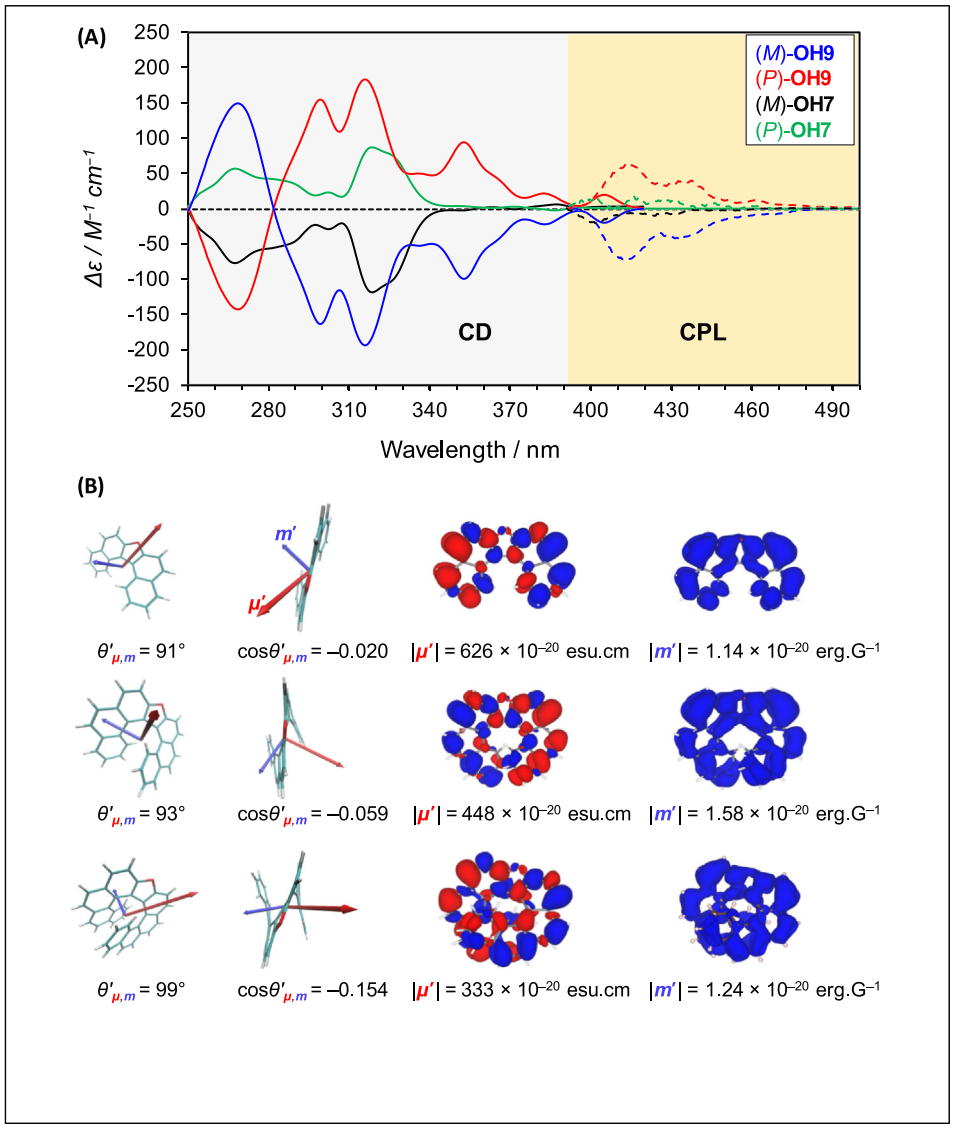

FIGURE 6 Chiroptical properties of oxa[*n*]helicenes: (A) CD (solid line) and CPL spectra (dashed line) of (*M*)-**OH9** (blue), (*P*)-**OH9** (red), (*M*)-**OH7** (black), (*P*)-**OH7** (green), studied in chloroform (Conc = 1×10^{-5} M); (B) the transition electric|μ'|(red), and magnetic|m'|(blue) dipole moment (TEDM) & (TMDM) densities for the $S_1 \rightarrow S_0$ transition of (*M*)-**OH5**, (*M*)-**OH7**, and (*M*)-**OH9** calculated at the MN15/6-311G(d,p)/PCM = chloroform level of theory (isosurface value: 0.003 a.u.). the length of vectors is amplified for clarity.

TABLE 1 Chiroptical features of (*M*)-**OH5**, (*M*)-**OH7**, and (*M*)-**OH9**.

	CD		$S_1 \rightarrow S_0$ transition						CPL	
	λ (nm)	g_{abs} (10^{-3})	|μ|(10^{-20} esu cm)[a]	|m|(10^{-20} erg G^{-1})[b]	$\theta_{\mu,m}$ (deg)[c]	cos ($\theta_{\mu,m}$)	(R) (10^{-40} (erg esu cm G^{-1})[d]	g_{cal}[e] (10^{-3})	λ_{em} (nm)	g_{lum}[e] (10^{-3})
(*M*)-**OH5**	-	-	625.61	1.14	91°	−0.020	−14.64	−0.15	-	-
(*M*)-**OH7**	319	4.6	447.53	1.58	93°	−0.059	−41.46	−0.83	402	−0.81
(*M*)-**OH9**	316	8.0	333.30	1.24	99°	−0.154	−63.44	−2.28	413	−2.20

[a]Electric transition dipole moments (ETDM) for the $S_1 \rightarrow S_0$ transitions. [b] Magnetic transition dipole moments (MTDM) for the $S_1 \rightarrow S_0$ transitions. [c] The angle between ETDM and MTDM vectors. [d] Rotational strength. [e] Dimensionless values.

typically much lower than the|μ|value (Table 1). The above equation can thus be simplified as $g_{lum} = 4 \cos \theta|m|/|\mu|$. The lower |μ|and larger cos θ of **OH9** than of **OH7** lead to a three-fold increase in the calculated luminescence dissymmetry factor (g_{cal}) (Table 1), consistent with the trend observed experimentally (Figure 6A). Similarly, **OH5** exhibited a parallel pattern in the calculations, featuring a lower|m|, higher|μ|, and a smaller (θ) of only 91°, (cosθ very close to zero). These factors collectively led to a significant drop in the calculated dissymmetry factor|g_{cal}|of **OH5** compared to **OH7** and **OH9** (Table 1). The comprehensive understanding of the

influence of helical extension on chiroptical features of oxa[*n*]helicenes, provides a valuable roadmap for designing chiral emitters that seamlessly integrate the ease of enantioselective synthesis (through their well-established chemistry) with the superior optical performance.[75]

The concept of fluorescence brightness has recently been extended to include CPL emitters, introducing the CPL brightness (B_{CPL}) as a metric for evaluating their overall performance (eq. 2), where the (ε_λ) is the molar extinction coefficient measured at the excitation wavelength.[76]

$$B_{CPL} = \varepsilon_\lambda . \Phi_f . \frac{g_{lum}}{2} \quad (2)$$

With the chiroptical results and Φ_f in hand, the B_{CPL} values of both **OH7** and **OH9** were calculated to be 1.35 M^{-1} cm^{-1}. This finding can be interpreted in the context of each one having a distinct advantage over the other: **OH9** exhibits higher (× 3 times) g_{lum}, while **OH7** demonstrates a higher (× 3 times) quantum yield (further details in Table S26, ESI).

4 | CONCLUSION

In conclusion, our investigation into the impact of helical extension on a series of symmetric oxa[*n*]helicenes (n = 5–9) provided comprehensive insights into their structural, photophysical, and chiroptical features. The single crystal X-ray analysis unveiled structural variations accompanying helical extension, influencing torsion angles, helical pitch, and packing arrangements dominated by C–H···π interactions. NICS calculations revealed a progressive augmentation in the aromaticity of terminal benzene rings with helical elongation, while the aromaticity of central furan rings decreased due to planarity distortion. Furthermore, the extended helicity induced red-shifted absorption and emission bands. Our TD-DFT calculations demonstrated a decrease in HOMO/LUMO gaps with helical extension, resulting in a reduction of optical bandgaps (E_g) to 3.02 eV for **OH9**, compared to 3.44 eV for **OH5**. The fluorescence quantum yields of **OH5** (Φ_f = 10.7%) and **OH7** (Φ_f = 11.2%) were three times higher than that of **OH9** (Φ_f = 3.8%). Calculated enantiomerization barriers of **OH5**, **OH7**, and **OH9** (3.18, 33.56, and 44.46 kcal mol^{-1}, respectively) underscored the significant influence of helical π-extension on backbone rigidity.

A slight variation in the main helical scaffold from (n = 7) to (n = 9) induced an approximately three-fold increase in dissymmetry factors, with the largest values of|g_{lum}|observed in **OH9** (2.2×10^{-3}) compared to **OH7** (0.8×10^{-3}). The lower|μ|and larger θ of **OH9** than **OH7** led to this three-fold increase. Finally, the B_{CPL} values of both **OH7** and **OH9** were calculated to be 1.35 M^{-1} cm^{-1} as each one shows a distinct advantage over the other. These findings collectively highlight the profound impact of helical extension on the structural and (chir)optical properties of oxa[*n*]helicenes. Further investigations for higher and unsymmetrical hetero[*n*]helicenes are currently under investigation.

AUTHOR CONTRIBUTIONS

Mohamed S. H. Salem: Conceptualization; data curation; formal analysis; investigation; methodology; project administration; software; visualization; writing—original draft. **Rubal Sharma:** Formal analysis; methodology; investigation; validation. **Seika Suzuki:** Formal analysis; visualization. **Yoshitane Imai:** Resources; visualization. **Mitsuhiro Arisawa:** Supervision. **Shinobu Takizawa:** Supervision; project administration; funding acquisition; conceptualization.

ACKNOWLEDGMENTS

We thank Yazan Alkatshah for helping with AICD plots during studying the aromaticity. We acknowledge the technical staff of the Comprehensive Analysis Center of SANKEN, Osaka University. The computational part was performed at the Research Center for Computational Science, Okazaki (IMS-RCCSA-ja & IMS-RCCS-mo-ja). This work was supported by JSPS KAKENHI Grants 24K17681, 21A204, 21H05217, and 22K06502 from the Ministry of Education, Culture, Sports, Science, and Technology (MEXT), the Japan Society for the Promotion of Science (JSPS), Core Research for Evolutionary Science and Technology (JST CREST) (No. JPMJCR20R1), and Hoansha Foundation.

DATA AVAILABILITY STATEMENT

Data are available on request from the corresponding authors.

ORCID

Mohamed S. H. Salem https://orcid.org/0000-0002-8919-095X
Rubal Sharma https://orcid.org/0009-0003-7827-882X
Shinobu Takizawa https://orcid.org/0000-0002-9668-1888

REFERENCES

1. Gingras M. One hundred years of helicene chemistry. Part 3: applications and properties of carbohelicenes. *Chem Soc Rev*. 2013;42(3):1051-1095. doi:10.1039/C2CS35134J
2. Shen Y, Chen C-F. Helicenes: synthesis and applications. *Chem Rev*. 2012;112(3):1463-1535. doi:10.1021/cr200087r

3. Jakubec M, Storch J. Recent advances in functionalizations of helicene backbone. *J Org Chem*. 2020;85(21):13415-13428. doi:10.1021/acs.joc.0c01837
4. Zhao W-L, Li M, Lu H-Y, Chen C-F. Advances in helicene derivatives with circularly polarized luminescence. *Chem Commun*. 2019;55(92):13793-13803. doi:10.1039/C9CC06861A
5. Cei M, Di Bari L, Zinna F. Circularly polarized luminescence of helicenes: a data-informed insight. *Chirality*. 2023;35(4):192-210. doi:10.1002/chir.23535
6. Khalid MI, Salem MSH, Takizawa S. Synthesis and structural and optical behavior of dehydrohelicene-containing polycyclic compounds. *Molecules*. 2024;29(2):296. doi:10.3390/molecules29020296
7. Anichini C, Czepa W, Pakulski D, Aliprandi A, Ciesielski A, Samorì P. Chemical sensing with 2d materials. *Chem Soc Rev*. 2018;47(13):4860-4908. doi:10.1039/C8CS00417J
8. Reetz MT, Sostmann S. 2, 15-dihydroxy-hexahelicene (helixol): synthesis and use as an enantioselective fluorescent sensor. *Tetrahedron*. 2001;57(13):2515-2520. doi:10.1016/S0040-4020(01)00077-1
9. Shen C, Loas G, Srebro-Hooper M, et al. Iron alkynyl helicenes: redox-triggered chiroptical tuning in the ir and near-ir spectral regions and suitable for telecommunications applications. *Angew Chem Int Ed*. 2016;55(28):8062-8066. doi:10.1002/anie.201601633
10. Kim D-Y. Potential application of spintronic light-emitting diode to binocular vision for three-dimensional display technology. *J Korean Phys Soc*. 2006;49:505-508.
11. Rocker J, Dresel JA, Krieger LA, et al. Substitution effects on the photophysical and photoredox properties of tetraaza[7]helicenes. *Chem a Eur J*. 2023;29(48):e202301244. doi:10.1002/chem.202301244
12. Usui K, Narita N, Eto R, et al. Oxidation of an internal-edge-substituted [5]helicene-derived phosphine synchronously enhances circularly polarized luminescence. *Chem a Eur J*. 2022;28(65):e202202922. doi:10.1002/chem.202202922
13. Mahato B, Panda AN. Effect of terminal fluorination on chiroptical properties of carbo[5–8]helicenes: a systematic computational study at the ri-adc (2) level. *J Phys Chem a*. 2023;127(10):2284-2294. doi:10.1021/acs.jpca.2c08474
14. Suzuki K, Fukuda H, Toda H, et al. Substituent effects on helical structures and chiroptical properties of fused anthracenes with bulky phenyl groups. *Tetrahedron*. 2023;132:133243. doi:10.1016/j.tet.2022.133243
15. Sakai H, Kubota T, Yuasa J, et al. Synthetic control of photophysical process and circularly polarized luminescence of [5]carbohelicene derivatives substituted by maleimide units. *J Phys Chem C*. 2016;120(14):7860-7869. doi:10.1021/acs.jpcc.6b01344
16. Yamamoto Y, Sakai H, Yuasa J, et al. Synthetic control of the excited-state dynamics and circularly polarized luminescence of fluorescent "push–pull" tetrathia[9]helicenes. *Chem a Eur J*. 2016;22(12):4263-4273. doi:10.1002/chem.201504048
17. Hong J, Xiao X, Liu H, et al. Controlling the emissive, chiroptical, and electrochemical properties of double [7] helicenes through embedded aromatic rings. *Chem a Eur J*. 2022;28(58):e202202243. doi:10.1002/chem.202202243
18. Appiarius Y, Míguez-Lago S, Puylaert P, et al. Boosting quantum yields and circularly polarized luminescence of penta-and hexahelicenes by doping with two bn-groups. *Chem Sci*. 2024;15(2):466-476. doi:10.1039/D3SC02685J
19. Li J-K, Chen X-Y, Guo Y-L, et al. B,N-embedded double hetero [7]helicenes with strong chiroptical responses in the visible light region. *J am Chem Soc*. 2021;143(43):17958-17963. doi:10.1021/jacs.1c09058
20. Salem MSH, Sharma R, Khalid MI, et al. Data-driven electrochemical one-pot synthesis of double hetero[7]dehydrohelicene. *Electrochemistry*. 2023;91(11):112015, 23-67092-112015. doi:10.5796/electrochemistry.23-67092
21. Hasegawa M, Nojima Y, Nagata Y, Usui K, Sugiura K, Mazaki Y. Synthesis and chiroptical properties of binaphthyl-hinged [5]helicenes. *Eur J Org Chem*. 2023;26:e202300656.
22. Zhou F, Huang Z, Huang Z, Cheng R, Yang Y, You J. Triple oxa[7]helicene with circularly polarized luminescence: enhancing the dissymmetry factors via helicene subunit multiplication. *Org Lett*. 2021;23(12):4559-4563. doi:10.1021/acs.orglett.1c01212
23. Tanaka H, Ikenosako M, Kato Y, Fujiki M, Inoue Y, Mori T. Symmetry-based rational design for boosting chiroptical responses. *Commun Chem*. 2018;1(1):38. doi:10.1038/s42004-018-0035-x
24. Full J, Wildervanck MJ, Dillmann C, et al. Impact of truncation on optoelectronic properties of azaborole helicenes. *Chem a Eur J*. 2023;29(70):e202302808. doi:10.1002/chem.202302808
25. Cruz CM, Castro-Fernández S, Maçôas E, Cuerva JM, Campaña AG. Undecabenzo[7]superhelicene: a helical nanographene ribbon as a circularly polarized luminescence emitter. *Angew Chem Int Ed*. 2018;57(45):14782-14786. doi:10.1002/anie.201808178
26. Niu W, Fu Y, Qiu Z-L, et al. π-Extended helical multilayer nanographenes with layer-dependent chiroptical properties. *J am Chem Soc*. 2023;145(49):26824-26832. doi:10.1021/jacs.3c09350
27. Mahato B, Panda AN. Effects of heterocyclic ring fusion and chain elongation on chiroptical properties of polyaza[9]helicene: a computational study. *J Phys Chem a*. 2022;126(8):1412-1421. doi:10.1021/acs.jpca.2c00432
28. Nakai Y, Mori T, Inoue Y. Theoretical and experimental studies on circular dichroism of carbo[*n*]helicenes. *J Phys Chem a*. 2012;116(27):7372-7385. doi:10.1021/jp304576g
29. Duan C, Zhang J, Xiang J, Yang X, Gao X. Azulene-embedded [*n*]helicenes (*n*= 5, 6 and 7). *Angew Chem Int Ed*. 2022;61(18):e202201494. doi:10.1002/anie.202201494
30. Shen C, Srebro-Hooper M, Jean M, et al. Synthesis and chiroptical properties of hexa-, octa-, and deca-azaborahelicenes: influence of helicene size and of the number of boron atoms. *Chem a Eur J*. 2017;23(2):407-418. doi:10.1002/chem.201604398
31. Duwald R, Pascal S, Bosson J, et al. Enantiospecific elongation of cationic helicenes by electrophilic functionalization at terminal ends. *Chem a Eur J*. 2017;23(55):13596-13601. doi:10.1002/chem.201703441
32. Tan J, Xu X, Liu J, et al. Synthesis of a π-extended double [9]helicene. *Angew Chem Int Ed*. 2023;62(18):e202218494. doi:10.1002/anie.202218494
33. Tian X, Shoyama K, Mahlmeister B, Brust F, Stolte M, Würthner F. Naphthalimide-annulated [*n*]helicenes: red circularly polarized light emitters. *J am Chem Soc*. 2023;145(17):9886-9894. doi:10.1021/jacs.3c03441

34. Qiu Z, Ju C-W, Frédéric L, et al. Amplification of dissymmetry factors in π-extended [7]- and [9]helicenes. *J am Chem Soc*. 2021;143(12):4661-4667. doi:10.1021/jacs.0c13197
35. Full F, Wölflick Q, Radacki K, Braunschweig H, Nowak-Król A. Enhanced optical properties of azaborole helicenes by lateral and helical extension. *Chem a Eur J*. 2022;28(62): e202202280. doi:10.1002/chem.202202280
36. Izquierdo-García P, Fernández-García JM, Medina Rivero S, et al. Helical bilayer nanographenes: impact of the helicene length on the structural, electrochemical, photophysical, and chiroptical properties. *J am Chem Soc*. 2023;145(21):11599-11610. doi:10.1021/jacs.3c01088
37. Sundararaghavan V, Varshney V, Simone D. Computational study of optical absorption spectra of helicenes as applied to strain sensing. *arXiv preprint arXiv:2303.03490* 2023.
38. Si Y, Cheng Y, Qu N, Zhao X, Yang G. Theoretical study on the photophysical properties of boron-fused double helicenes. *RSC Adv*. 2017;7(89):56543-56549. doi:10.1039/C7RA11476A
39. Sako M, Takeuchi Y, Tsujihara T, et al. Efficient enantioselective synthesis of oxahelicenes using redox/acid cooperative catalysts. *J am Chem Soc*. 2016;138(36):11481-11484. doi:10.1021/jacs.6b07424
40. Kumar A, Sasai H, Takizawa S. Atroposelective synthesis of C–C axially chiral compounds via mono-and dinuclear vanadium catalysis. *Acc Chem Res*. 2022;55(20):2949-2965. doi:10.1021/acs.accounts.2c00545
41. Khalid MI, Salem MSH, Sako M, Kondo M, Sasai H, Takizawa S. Electrochemical synthesis of heterodehydro[7]helicenes. *Commun Chem*. 2022;5(1):166. doi:10.1038/s42004-022-00780-7
42. Salem MSH, Khalid MI, Sako M, et al. Electrochemical synthesis of hetero[7]helicenes containing pyrrole and furan rings *via* an oxidative heterocoupling and dehydrative cyclization sequence. *Adv Synth Catal*. 2023;365(3):373-380. doi:10.1002/adsc.202201262
43. Kamble GT, Salem MSH, Abe T, et al. Chiral vanadium (v)-catalyzed oxidative coupling of 4-hydroxycarbazoles. *Chem Lett*. 2021;50(10):1755-1757. doi:10.1246/cl.210367
44. Chang H, Liu H, Dmitrieva E, et al. Furan-containing double tetraoxa[7]helicene and its radical cation. *Chem Commun*. 2020;56(96):15181-15184. doi:10.1039/D0CC06970A
45. Sundar MS, Bedekar AV. Synthesis and study of 7, 12, 17-trioxa [11]helicene. *Org Lett*. 2015;17(23):5808-5811. doi:10.1021/acs.orglett.5b02948
46. Matsuno T, Koyama Y, Hiroto S, Kumar J, Kawai T, Shinokubo H. Isolation of a 1,4-diketone intermediate in oxidative dimerization of 2-hydroxyanthracene and its conversion to oxahelicene. *Chem Commun*. 2015;51(22):4607-4610. doi:10.1039/C5CC00764J
47. Frisch MJ, Trucks GW, Schlegel HB, et al. *Gaussian 09, revision D.1*. Gaussian, Inc.; 2013.
48. Frisch M, Trucks G, Schlegel HB, et al. *Gaussian 16*. Gaussian, Inc.; 2016.
49. Haoyu SY, He X, Li SL, Truhlar DG. Mn15: a kohn–sham global-hybrid exchange–correlation density functional with broad accuracy for multi-reference and single-reference systems and noncovalent interactions. *Chem Sci*. 2016;7(8):5032-5051. doi:10.1039/C6SC00705H
50. Schleyer PVR, Maerker C, Dransfeld A, Jiao H, van Eikema Hommes NJ. Nucleus-independent chemical shifts: a simple and efficient aromaticity probe. *J am Chem Soc*. 1996;118(26): 6317-6318. doi:10.1021/ja960582d
51. Chen Z, Wannere CS, Corminboeuf C, Puchta R, Schleyer PVR. Nucleus-independent chemical shifts (NICS) as an aromaticity criterion. *Chem Rev*. 2005;105(10):3842-3888. doi:10.1021/cr030088+
52. McLean A, Chandler G. Contracted gaussian basis sets for molecular calculations. I. Second row atoms, z= 11–18. *J Chem Phys*. 1980;72(10):5639-5648. doi:10.1063/1.438980
53. Geuenich D, Hess K, Köhler F, Herges R. Anisotropy of the induced current density (ACID), a general method to quantify and visualize electronic delocalization. *Chem Rev*. 2005; 105(10):3758-3772. doi:10.1021/cr0300901
54. Salem MSH, Sabri A, Khalid MI, Sasai H, Takizawa S. Two-step synthesis, structure, and optical features of a double hetero[7] helicene. *Molecules*. 2022;27(24):9068. doi:10.3390/molecules27249068
55. Casida ME, Huix-Rotllant M. Progress in time-dependent density-functional theory. *Annu Rev Phys Chem*. 2012;63(1): 287-323. doi:10.1146/annurev-physchem-032511-143803
56. Lu T, Chen F. Multiwfn: a multifunctional wavefunction analyzer. *J Comput Chem*. 2012;33(5):580-592. doi:10.1002/jcc.22885
57. Humphrey W, Dalke A, Schulten K. Vmd: visual molecular dynamics. *J Mol Graph*. 1996;14(1):33-38. doi:10.1016/0263-7855(96)00018-5
58. Nakanishi K, Fukatsu D, Takaishi K, et al. Oligonaphthofurans: fan-shaped and three-dimensional π-compounds. *J am Chem Soc*. 2014;136(19):7101-7109. doi:10.1021/ja502209w
59. Nakano K, Hidehira Y, Takahashi K, Hiyama T, Nozaki K. Stereospecific synthesis of hetero[7]helicenes by Pd-catalyzed double *N*-arylation and intramolecular *O*-arylation. *Angew Chem Int Ed*. 2005;44(43):7136-7138. doi:10.1002/anie.200502855
60. Johnson CE Jr, Bovey F. Calculation of nuclear magnetic resonance spectra of aromatic hydrocarbons. *J Chem Phys*. 1958; 29(5):1012-1014. doi:10.1063/1.1744645
61. Krygowski T, Cyranski M, Czarnocki Z, Häfelinger G, Katritzky AR. Aromaticity: a theoretical concept of immense practical importance. *Tetrahedron*. 2000;56(13):1783-1796. doi:10.1016/S0040-4020(99)00979-5
62. Nakakuki Y, Hirose T, Sotome H, Miyasaka H, Matsuda K. Hexa-*peri*-hexabenzo[7]helicene: homogeneously π-extended helicene as a primary substructure of helically twisted chiral graphenes. *J am Chem Soc*. 2018;140(12):4317-4326. doi:10.1021/jacs.7b13412
63. Kubo H, Hirose T, Nakashima T, Kawai T, Hasegawa J-Y, Matsuda K. Tuning transition electric and magnetic dipole moments:[7] helicenes showing intense circularly polarized luminescence. *J Phys Chem Lett*. 2021;12(1):686-695. doi:10.1021/acs.jpclett.0c03174
64. Kubo H, Shimizu D, Hirose T, Matsuda K. Circularly polarized luminescence designed from molecular orbitals: a figure-eight-shaped [5] helicene dimer with D_2 symmetry. *Org Lett*. 2020;22(23):9276-9281. doi:10.1021/acs.orglett.0c03506
65. Sapir M, Vander DE. Intersystem crossing in the helicenes. *Chem Phys Lett*. 1975;36(1):108-110. doi:10.1016/0009-2614(75)85698-3

66. Hirose T, Tsunoi Y, Fujimori Y, Matsuda K. Fluorescence enhancement of covalently linked 1-cyano-1,2-diphenylethene chromophores with naphthalene-1,8-diyl linker units: analysis based on kinetic constants. *Chem a Eur J*. 2015;21(4):1637-1644. doi:10.1002/chem.201404745
67. Lehtonen O, Sundholm D, Vänskä T. Computational studies of semiconductor quantum dots. *Phys Chem Chem Phys*. 2008;10(31):4535-4550. doi:10.1039/b804212h
68. Salem MSH, Khalid MI, Sasai H, Takizawa S. Two-pot synthesis of unsymmetrical hetero[7]helicenes with intriguing optical properties. *Tetrahedron*. 2023;133:133266. doi:10.1016/j.tet.2023.133266
69. Barroso J, Cabellos JL, Pan S, et al. Revisiting the racemization mechanism of helicenes. *Chem Commun*. 2018;54(2):188-191. doi:10.1039/C7CC08191J
70. Hossain MS, Akter M, Shahabuddin M, Salim M, Iimura K-I, Karikomi M. Synthesis of enantiomerically pure oxa[9]helicene derivatives by a nucleophilic cyclodehydration reaction of helical 1,1′-bibenzo[*c*]phenanthrenylidene-2, 2′-dione. *Synlett*. 2022;33(3):277-282. doi:10.1055/a-1684-0448
71. Schellman JA. Circular dichroism and optical rotation. *Chem Rev*. 1975;75(3):323-331. doi:10.1021/cr60295a004
72. Warnke I, Furche F. Circular dichroism: Electronic. *Wiley Interdiscip Rev Comput Mol Sci*. 2012;2(1):150-166. doi:10.1002/wcms.55
73. Guido CA, Zinna F, Pescitelli G. CPL calculations of [7]helicenes with alleged exceptional emission dissymmetry values. *J Mater Chem C*. 2023;11(31):10474-10482. doi:10.1039/D3TC01532G
74. Guo SM, Huh S, Coehlo M, Shen L, Pieters G, Baudoin O. A C–H activation-based enantioselective synthesis of lower carbo [*n*]helicenes. *Nat Chem*. 2023;15(6):872-880. doi:10.1038/s41557-023-01174-5
75. Mori T. Chiroptical properties of symmetric double, triple, and multiple helicenes. *Chem Rev*. 2021;121(4):2373-2412. doi:10.1021/acs.chemrev.0c01017
76. Arrico L, Di Bari L, Zinna F. Quantifying the overall efficiency of circularly polarized emitters. *Chem a Eur J*. 2021;27(9):2920-2934. doi:10.1002/chem.202002791

SUPPORTING INFORMATION

Additional supporting information can be found online in the Supporting Information section at the end of this article.

How to cite this article: Salem MSH, Sharma R, Suzuki S, Imai Y, Arisawa M, Takizawa S. Impact of helical elongation of symmetric oxa[*n*]helicenes on their structural, photophysical, and chiroptical characteristics. *Chirality*. 2024;36(5):e23673. doi:10.1002/chir.23673